Kinetic Characterization of Strongly Coupled Systems

C. A. Knapek,[1,*] A. V. Ivlev,[1] B. A. Klumov,[1] G. E. Morfill,[1] and D. Samsonov[2]
[1]*Max-Planck-Institute for Extraterrestrial Physics, 85741 Garching, Germany*
[2]*Department of Electrical Engineering and Electronics, The University of Liverpool, Liverpool L69 3GJ, United Kingdom*
(Received 7 September 2006; published 3 January 2007)

We propose a simple method to determine the local coupling strength Γ experimentally, by linking the individual particle dynamics with the local density and crystal structure of a 2D plasma crystal. By measuring particle trajectories with high spatial and temporal resolution we obtain the first maps of Γ and temperature at individual particle resolution. We employ numerical simulations to test this new method, and discuss the implications to characterize strongly coupled systems.

DOI: 10.1103/PhysRevLett.98.015001 PACS numbers: 52.27.Lw, 05.70.−a, 61.50.−f

There are numerous phenomena occurring in strongly coupled media that are known or (at least) believed to be strongly dependent on the local variations of the parameters of state (e.g., local density, temperature, order parameter). These are, e.g., nonequilibrium phase transitions [1], annealing and glass transitions [2], interfacial melting and growth of nanoclusters and crystals [3,4], formation of plasma crystals [5–7], etc. One of the most important parameters characterizing the local state of the medium is the interaction (coupling, binding) strength, the local ratio of the pair interaction potential to the kinetic energy Γ. Complex plasmas allow detailed spatial and temporal measurements to be made at the characteristic system length and time scales. The coupling strength for these systems is determined by the electrostatic (Madelung) energy of the interparticle interaction. Transitions between solid and fluid phases as well as between different crystalline states [8], rheological and transport properties of the fluid phase [9], energy relaxation and hierarchy of metastable states [10] in complex plasmas are determined by the magnitude of the coupling strength. In turn the coupling strength depends sensitively on local variations in crystal structure, caused by defects, boundaries, doping, etc., and provides information about the occurrence of localized excited states and nonstationary processes.

In this Letter we propose a simple method to determine Γ experimentally, by linking the individual particle dynamics with the local density and crystal structure using the Einstein frequency Ω_E, which refers to linear oscillations of individual particles (atoms) in a lattice [11]. By measuring individual particle trajectories in a 2D plasma crystal with high spatial and temporal resolution we have obtained the first maps of Γ and temperature T at individual particle resolution. We employ numerical simulations to test this new method, and discuss the implications to characterize strongly coupled systems.

We calculate the "plasma crystal Einstein (PCE) frequency" for different lattices. By dividing the lattice around a test particle of charge Q into concentric circles (2D) or spheres (3D) ("shells") with the center at $\mathbf{r} = 0$, so that the first shell contains the nearest neighbors, the second shell the next $+1$ set of particles, and so on. Assuming isotropic interaction via a potential ϕ, the potential energy of the particle displacement can be written as $W(\mathbf{r}) = \sum_{\text{shells}} \sum_i Q\phi(R_i)$ (for simplicity, we omit indexing of shells). Summation over i accounts for the interaction with all particles of a given shell, $R_i^2 = R^2 + r^2 + 2Rr\cos\chi_i$ with R the shell radius and χ_i the angle between $\mathbf{r}$ and $R\mathbf{n}_i$ (directed towards the ith particle). Also, $\cos\chi_i = \cos\theta\cos\theta_i + \sin\theta\sin\theta_i\cos(\varphi - \varphi_i)$, where (θ, φ) are the spherical coordinates of $\mathbf{r}$ and (θ_i, φ_i) of $\mathbf{n}_i$. Taking into account the equilibrium condition $(dW/dr)|_{r=0} = 0$, expansion over $\mathbf{r}$ yields $W = W_0 + \frac{1}{2}m\Omega_E^2 r^2 + o(r^2)$ where m is the particle mass. Assuming a Yukawa potential $\phi(R) = (Q/R)e^{-K}$ [10,12,13] with the screening length λ and $K = R/\lambda$ we obtain for the PCE frequency

$$\Omega_E^2 = \frac{Q^2}{m\lambda^3}\sum_{\text{shells}}\frac{e^{-K}}{K} \times \sum_i [(1 + 3K^{-1} + 3K^{-2})\cos^2\chi_i - K^{-1} - K^{-2}], \quad (1)$$

where $\cos^2\chi_i = \cos^2\theta\cos^2\theta_i + \frac{1}{2}\sin^2\theta\sin^2\theta_i$ (here the equilibrium condition was used). Particles with isotropic Yukawa interaction (as well as with other types of short- and long-range isotropic interaction) usually arrange themselves into lattices with "even" distribution, so that Ω_E does not depend on the angle(s) [8,10]: In 3D, particles form either cubic lattices (bcc and fcc) or volume hexagonal structures (hcp or random hcp, both are metastable), and in 2D they form a planar hexagonal lattice. Note that for 1D chains Ω_E can be naturally obtained from Eq. (1) by setting $\cos\chi_i = \pm 1$.

By normalizing the PCE frequency to the one-component-plasma (OCP) scale $\Omega_0 = (Q^2/m\Delta^3)^{1/2}$ (where Δ is the nearest-neighbor distance in a crystal), we find that the ratio $\Omega_E/\Omega_0 \equiv f(\kappa)$ depends only on the screening parameter $\kappa = \Delta/\lambda$. This "κ factor" $f(\kappa)$ is plotted in Fig. 1. For reference, we also show the frequency of a 1D chain. It is remarkable that the frequencies of 2D hexagonal and 3D bcc lattices practically coincide. Also, the fcc and hcp branches are so close that they cannot be distinguished. The difference between bcc and fcc or hcp branches is small. The inset in Fig. 1 demonstrates that the role of

 © 2007 The American Physical Society

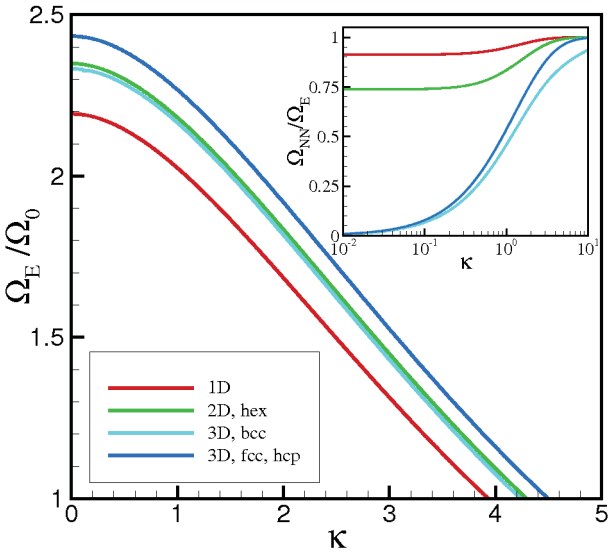

FIG. 1 (color). Plasma crystal Einstein (PCE) frequency Ω_E normalized to $\Omega_0 = (Q^2/m\Delta^3)^{1/2}$ versus screening parameter $\kappa = \Delta/\lambda$, as calculated from Eq. (1). Plotted curves are for 1D chain, 2D hexagonal lattice, and 3D bcc, fcc, and hcp lattices. The inset shows the ratio of frequency Ω_{NN} calculated in the nearest-neighbor approximation to the PCE frequency. $(\Omega_{NN}/\Omega_0)^2$ in dependence on κ is $4e^{-\kappa}(1+\kappa+\frac{1}{2}\kappa^2)$ (1D chain), $3e^{-\kappa}(1+\kappa+\kappa^2)$ (2D hexagonal lattice), $\frac{8}{3}e^{-\kappa}\kappa^2$ (3D bcc lattice) and $4e^{-\kappa}\kappa^2$ (3D fcc, hcp, and random hcp lattices).

interaction with particles beyond the nearest-neighbor shell increases as the dimensionality grows: While for a 1D chain the nearest-neighbor approximation is reasonable at practically any κ, for 3D lattices the inclusion of next shells is necessary even if κ significantly exceeds unity. The reason is that the distance between consecutive shells in 3D lattices can be rather small [for instance, the distance between the nearest-neighbor and the second shells in the bcc lattice is $(\frac{2}{\sqrt{3}}-1)\Delta \simeq 0.15\Delta$]. This fact might play a very important role when studying, e.g., particle dynamics in nanocrystallites, nanodomains, and clusters, where the influence of edge effects is significant.

Microparticles embedded in a neutral gas acquire the kinetic temperature of the neutrals. In a partially ionized plasma the microparticles become charged, their interaction with the plasma particles (ions and electrons) provides an additional source of energy and, hence, their kinetic temperature is not necessarily equal to the neutral gas temperature [12]. In local equilibrium, when the interaction with the plasma as well as with individual neutral atoms is, on average, balanced by neutral friction, the dynamics of individual particles in the lattice can, in principle, be described by a Langevin equation [14]. The particle ensemble should obey the Maxwell-Boltzmann distribution, so that for each lattice cell one can write the probability distribution

$$P(\mathbf{r},\mathbf{v}) \propto \exp\left[-\frac{m(\mathbf{v}-\langle\mathbf{v}\rangle)^2}{2T}-\frac{m\Omega_E^2 r^2}{2T}\right], \qquad (2)$$

with all $\mathbf{v}$ available in phase space and T is the particle temperature. For ergodic processes, the average over an ensemble is equivalent to the time average. Therefore, assuming that the ergodic hypothesis is applicable to equilibrium plasma crystals, the independent Gaussian fit of the velocity and displacement distribution for each individual particle can provide its (local) temperature and coupling parameter: The velocity dispersion is $\sigma_v^2 = T/m$ and the displacement dispersion is $\sigma_r^2 = T/m\Omega_E^2 \equiv \Delta^2/\tilde{\Gamma}$, where $\tilde{\Gamma} \equiv \Gamma f^2(\kappa)$, $\Gamma = Q^2/T\Delta$, is the effective coupling strength modified by the screening via the κ factor. It is essential that particles in the lattice perform sufficiently small oscillations, so that the role of anharmonic effects can be neglected. The linear harmonic oscillations of the neighboring particles are then uncoupled and can therefore be treated independently, which allows us to deduce local properties of the crystal (viz., T and $\tilde{\Gamma}$).

The experiment was performed in a weakly ionized argon plasma generated by a capacitively coupled rf discharge at 13.56 MHz between a horizontal lower electrode with a self-bias of -69 V and the grounded vacuum chamber walls. The setup was similar to the one used in [15]. The neutral gas pressure was 1.95 Pa. Melamine-formaldehyde spheres of 9.19 μm in diameter and a mass density of 1.51 g/cm^3 were electrostatically levitated in the plasma sheath $\approx$ 6.4 mm above the lower electrode and formed a 2D hexagonal lattice. No particles were located above or below this layer. Horizontal confinement was provided by a parabolic potential produced by a rim on the lower electrode, and by two parallel free floating wires mounted at the suspension level of the particles. Pressure and particle size yield a neutral drag (Epstein) coefficient of $\nu \simeq 2$ s^{-1}. A 532 nm Nd:YAG laser provided a laser sheet with a Gaussian vertical width of ≈ 200 μm which illuminated the crystal plane from the side. A high speed camera recorded 6144 images with 1024×1024 pixels from the top view at a frame rate of 500 frames per second and a spatial resolution of 6.74 μm/pixel. In total, 113 particles were observed in the field of view, with an average interparticle distance of $\Delta = 0.7$ mm. Wave spectra analysis [16] yielded a screening parameter $\kappa = 1$ with an accuracy of about 15%, and a mean particle charge of $Q \simeq 14\,000e$.

Coordinates of individual particles $\mathbf{R}_i$ were extracted from the images by an intensity weighting method. The velocity vector $\mathbf{v}_i = [\mathbf{R}_i(t+\delta t) - \mathbf{R}_i(t)]/\delta t$ was obtained by tracing each particle from frame to frame. Instead of the full frame rate of 500 fps as time step, only each third frame was used, since the spatial resolution of motion from frame to frame was in the range of the measurement uncertainty of 0.28 μm (random Gaussian pixel noise caused by the recording device). Therefore $\delta t = 6$ ms with an error in the velocity components due to pixel noise of 0.054 mm/s.

To analyze the individual particle motion, we introduced a local coordinate system in the reference frame of the

neighbors (with a time-dependent center, "mean lattice site") which allowed us to remove all systemic trends associated with a slow rigid-body drift of the crystal. This gives a time-dependent and localized mean interparticle distance $\Delta_i(t) = \frac{1}{n}\sum_{j=1}^{n} |\mathbf{R}_i(t) - \mathbf{R}_j(t)|$ and displacement $\mathbf{r}_i(t) = \{x_i(t), y_i(t)\} = \mathbf{R}_i(t) - \frac{1}{n}\sum_{j=1}^{n} \mathbf{R}_j(t)$ from the mean lattice site. The summation is over the nearest neighbors which were identified by performing Delauney triangulations. For the analysis we accepted only particles with $n = 6$ nearest neighbors. Two sample particle trajectories are shown in Figs. 2(c) and 2(f). The histograms of the velocity components $\{v_x, v_y\}$ of each particle were fitted to Maxwellian distributions (examples are shown in Figs. 2(a) and 2(d)], yielding the dispersions $\sigma^2_{v_x,i}$ and $\sigma^2_{v_y,i}$. In accordance with Eq. (2), the dispersion of the velocity distribution for the ith particle, $\sigma^2_{v,i} = (\sigma^2_{v_x,i} + \sigma^2_{v_y,i})/2$, yielded the "local" temperature T_i. Figure 3(a) shows that the distribution of T across the crystal is random within a range of 0.041–0.066 eV, slightly above room temperature, as expected.

To obtain the local coupling strength, we made Gaussian fits to the histograms of the displacement components $\{x, y\}$ [shown in Figs. 2(b) and 2(e)] and derived the displacement dispersion $\sigma^2_{r,i} = (\sigma^2_{x,i} + \sigma^2_{y,i})/2 \equiv \Delta_i^2/\tilde{\Gamma}_i$. Using the time-averaged mean local interparticle distance in the crystal Δ_i, we calculated $\tilde{\Gamma}_i = \Delta_i^2/\sigma^2_{r,i}$ as a local quantity. Figures 3(b) and 3(c) show the maps of $\tilde{\Gamma}$ and Δ, respectively. The Δ map reveals a density gradient, from left to right, which is caused by the weak horizontal compression produced by the wires. The influence of this gradient on $\tilde{\Gamma}$ is not noticeable. The *nonstationary* particle motion has the strongest influence on $\tilde{\Gamma}$: The region with lower $\tilde{\Gamma}$ at the upper edge of the crystal [Fig. 3(b)] coincides with a region of nonequilibrium particle redistribution, which occurred during the observation time. Although such nonstationary processes may have no (noticeable) impact on mean local T and Δ [see Figs. 3(a) and 3(c)], the obvious effect on the coupling strength indicates how sensitive this parameter reacts to nonequilibrium phenomena.

To identify the role of structural properties of the crystal, the bond order parameter Ψ_n [17] has been calculated, with n being the number of nearest neighbors. For a hexagonal order, $n = 6$ and $\Psi_6 = \frac{1}{6}|\langle\sum e^{6i\theta_j}\rangle|$ is equal to unity in a perfect (even) lattice, with θ_j being the angle between the nearest-neighbor-bond j and the x axis. The sum is taken over the six nearest neighbors, the angular brackets indicate an average over the time series for each particle. The map of the local bond order parameter is plotted in Fig. 3(d), all particles shown have six nearest neighbors. The origin of the anomaly seen in the bottom left corner is due to a sevenfold to fivefold pair defect (indicated by the circle). The hexagonal bond order reacts sensitively in the vicinity of the defect (as expected), whereas both the interparticle distance and the coupling parameter remain essentially unaffected [see Figs. 3(b) and 3(c)].

The coupling strength is related to the particle charge via $\tilde{\Gamma} = (Q^2/\Delta T) f^2(\kappa)$. Knowing $\tilde{\Gamma}$, T, and Δ from our measurement, and using the estimated screening length $\lambda = 0.7$ mm ($\kappa = 1$), we obtain a mean particle charge to be $Q \simeq 12\,000e$. Note that possible local variations of the charge, if any, have to be rather small: charge variations cause corresponding variations in the particle levitation height. Since all particles were observed within the illuminating laser sheet of $H_{\text{laser}} \simeq 100$ μm half-width, whereas the spatial scale of the vertical electric field, E, is about $H_{\text{field}} \simeq 2$ mm, we infer from $QE = mg$ that the relative charge variations must be smaller than $H_{\text{laser}}/H_{\text{field}} \simeq 5\%$.

We compared the experiment with molecular dynamics (MD) simulations which were performed for a two-dimensional system of Yukawa-interacting particles. The parameters were similar to those of the experiment (parti-

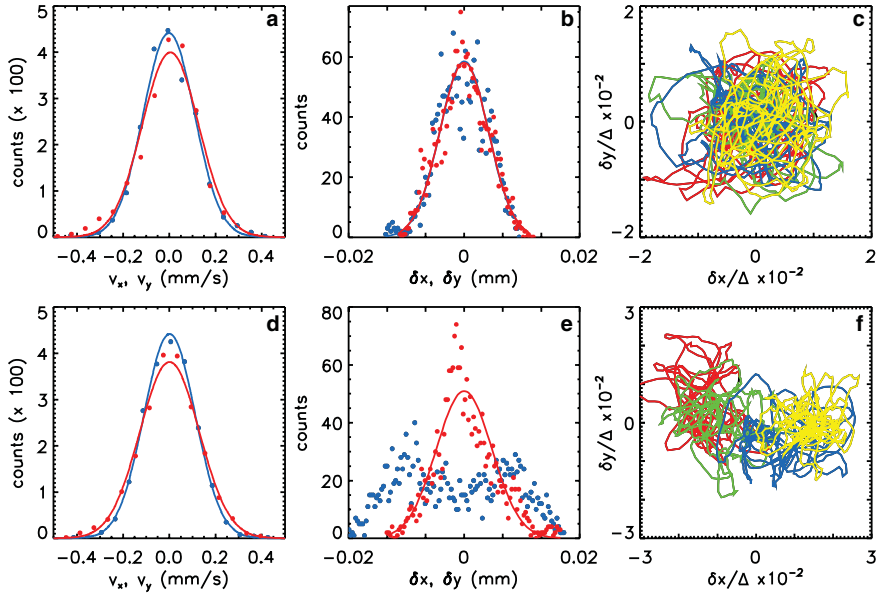

FIG. 2 (color). (a),(d) Distribution of velocities v_x (red dots) and v_y (blue dots) with Maxwellian fits (solid lines). (b),(e) Distribution of displacements x (red dots) and y (blue dots) of particles in their nearest-neighbor cage, solid lines are Gaussian fits. We chose the bin size of the histograms to be larger than the measurement error. (c),(f) Particle trajectories in their respective nearest-neighbor cells during the measurement time of $\simeq 12.3$ s (colors correspond to the progression of time). (a)–(c) [(d)–(f)] represent stationary (nonstationary) trajectories, respectively.

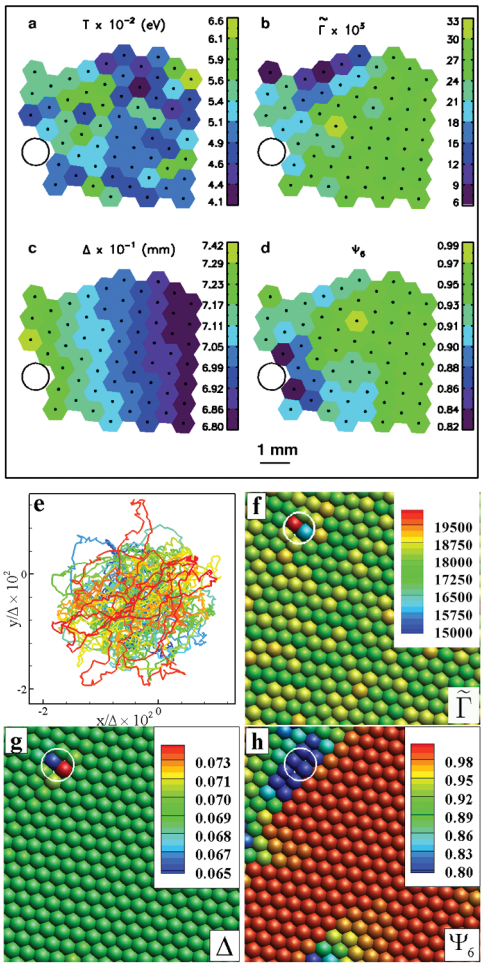

FIG. 3 (color). 2D maps of local crystal parameters. The voronoi cell around each particle is color coded according to the value of the particular measured quantity (the scales are shown in the bars on the right side of each picture). The circles indicate the position of the sevenfold to fivefold pair defect. Top panel: Experiment. (a) Particle temperature T, (b) coupling parameter $\tilde{\Gamma}$, (c) interparticle distance Δ, and (d) bond order parameter Ψ_6. Blue cells seen at the upper edge of Fig. 3(b) represent nonstationary particles, with a trajectory example shown in Fig. 2(f). The (compressing) wires are arranged along the vertical image axis to the left and right of the plasma crystal. Bottom panel: MD simulation. (e) Sample particle trajectory during $\simeq 10$ s, colors correspond to the time progression, (f) coupling parameter $\tilde{\Gamma}$, (g) interparticle distance Δ, (h) and bond order parameter Ψ_6.

cle size and density, mean interparticle distance, neutral gas density). Initially $N = 3600$ particles having a charge $Q = 10^4$ and an (average) screening parameter $\kappa = 1$ were randomly distributed over a square box of size $L = 2$ cm with periodic boundary conditions. The system quickly crystallized and the subsequent long-term behavior was studied in detail. Particle dynamics evolves according to the Langevin equation, with the Langevin forces defined by random Gaussian variables with a white spectrum [see Fig. 3(e) for a particle trajectory]. We show the computed two-dimensional distributions of time-averaged coupling strength $\tilde{\Gamma}$ [Fig. 3(f)], interparticle distance Δ [Fig. 3(g)], and bond orientational parameter Ψ_n [Fig. 3(h)]. The simulations confirm the experimental result that the sevenfold to fivefold pair defect (indicated by the circle in Fig. 3) has a well-pronounced long-range effect on the bond order, whereas $\tilde{\Gamma}$ and Δ have no visible signatures (outside the defect).

The presented analysis is essentially local, i.e., provided plasma variations occur on scales larger than Δ, and the results are not affected by such variations.

A kinetic theory of strongly coupled systems is notoriously difficult to develop. This is partly due to the self-organization, the long-range order, and the difficulty associated with identifying order parameters that characterize the various aspects of strong coupling phenomena. Based on our results it would appear that significant advances are possible using the local (kinetic) order parameters: dimensionless coupling strength Γ, dimensionless measure of lattice spacing or density κ, and orientational order Ψ_n. Note that all these quantities are scalars. For anisotropic systems, Γ and κ can, of course, also be computed in vector form, a route that might naturally lead to a kinetic theory of liquids. A straightforward application of the method described above is to determine the *local* Lindemann criterion of crystal melting, viz., what is the critical magnitude of the mean squared displacement, what are the characteristic patterns of the caged particle motion in the vicinity of the melting transition and what is the role of dynamical heterogeneity (e.g., dislocations, defects, grain boundaries).

*Electronic address: knapek@mpe.mpg.de

[1] G. Ódor, Rev. Mod. Phys. **76**, 663 (2004).
[2] H. W. Sheng *et al.*, Nature (London) **439**, 419 (2006).
[3] V. J. Anderson and H. N. W. Lekkerkerker, Nature (London) **416**, 811 (2002).
[4] F. Baletto and R. Ferrando, Rev. Mod. Phys. **77**, 371 (2005).
[5] H. Thomas, G. E. Morfill, and V. Demmel, Phys. Rev. Lett. **73**, 652 (1994).
[6] J. H. Chu and L. I, Phys. Rev. Lett. **72**, 4009 (1994).
[7] H. M. Thomas and G. E. Morfill, Nature (London) **379**, 806 (1996).
[8] S. Hamaguchi, R. T. Farouki, and D. H. E. Dubin, Phys. Rev. E **56**, 4671 (1997).
[9] G. Salin and J. H. Caillol, Phys. Rev. Lett. **88**, 065002 (2002).
[10] A. P. Nefedov *et al.*, New J. Phys. **5**, 33 (2003).
[11] C. Kittel, *Introduction to Solid State Physics* (Wiley, Toronto, 1976).
[12] V. E. Fortov *et al.*, Phys. Rep. **421**, 1 (2005).
[13] U. Konopka, G. E. Morfill, and L. Ratke, Phys. Rev. Lett. **84**, 891 (2000).
[14] R. A. Quinn and J. Goree, Phys. Rev. E **61**, 3033 (2000).
[15] S. Nunomura *et al.*, Phys. Rev. Lett. **95**, 025003 (2005).
[16] S. Nunomura *et al.*, Phys. Rev. E **65**, 066402 (2002).
[17] D. G. Grier and C. A. Murray, J. Chem. Phys. **100**, 9088 (1994).